

Attention-Enhanced Reservoir Computing

Felix Köster,* Kazutaka Kanno, Jun Ohkubo, and Atsushi Uchida†

*Department of Information and Computer Sciences, Saitama University
255 Shimo-Okubo, Sakura-ku, Saitama City, Saitama, 338-8570, Japan*

(Dated: December 29, 2023)

Photonic reservoir computing has been recently utilized in time series forecasting as the need for hardware implementations to accelerate these predictions has increased. Forecasting chaotic time series remains a significant challenge, an area where the conventional reservoir computing framework encounters limitations of prediction accuracy. We introduce an attention mechanism to the reservoir computing model in the output stage. This attention layer is designed to prioritize distinct features and temporal sequences, thereby substantially enhancing the forecasting accuracy. Our results show that a photonic reservoir computer enhanced with the attention mechanism exhibits improved forecasting capabilities for smaller reservoirs. These advancements highlight the transformative possibilities of reservoir computing for practical applications where accurate forecasting of chaotic time series is crucial.

I. INTRODUCTION

The combination of photonics and machine learning has emerged as a promising field of information processing, utilizing the development of more rapid and efficient computational methodologies [1]. Central to this interdisciplinary area is the concept of photonic reservoir computing, a paradigm that utilizes optic capabilities to enhance reservoir computations [2–9]. A semiconductor laser is one example of a photonic reservoir with optical feedback, which is a prime example of the photonic delay-based reservoir computer model [4–8]. Numerous studies have underscored the efficacy of delay-based reservoir computing in tackling a spectrum of complex tasks, extending from bit error correction [9] to spatiotemporal chaotic systems [10].

Chaotic time-series prediction is known to be challenging owing to its inherent sensitivity to accuracy and its pronounced nonlinearity [11]. A prime example of this challenge is weather forecasting, which is typically limited to short-term predictions due to the fundamentally chaotic nature of weather systems.

The framework of reservoir computing has been widely implemented using a variety of physical devices, such as electronic circuits [12], spintronic devices [13], soft robots [14], and nanostructure materials [15]. One of the advantages of reservoir computing is the easy implementation of the reservoir without high computational cost because input weights and network weights are randomly fixed, and only the output weights are trained by a learning algorithm. Classical reservoir computing is often limited because of the inflexibility of the fixed output structure when faced with the complexities inherent in such chaotic time series [16]. However, hardware technology advancements have opened pathways for accelerated forecasting, giving access to real-time responses and improved computational efficiency [17]. This progress has enabled the integration of reservoir computing with other advanced machine learning methods, one example being deep

learning and its most successful recent development, the attention mechanism [18].

To further enhance the predictive capabilities of reservoir computing, we propose integrating the attention mechanism within a reservoir computer. This mechanism has demonstrated superior effects in diverse areas of machine learning [18]. By incorporating an attention layer as the output layer, the system acquires the capacity to prioritize specific temporal characteristics, potentially yielding a more dynamic comprehension of the data [19].

This study introduces the attention mechanism to delay-based photonic reservoir computing using a semiconductor laser with optical feedback. We perform chaotic time series prediction by deploying two benchmark tasks. The first is the unidirectional coupling of two Lorenz systems, in which the reservoir computer is only exposed to the x , y , and z variables of the forced Lorenz system [20], while the driving system remains hidden, thus rendering the task a non-Markovian deterministic chaotic system with hidden states. The second is a time series consisting of alternating Lorenz and Rössler data sets [21], which we use to investigate how well the attention mechanism adapts to swiftly changing tasks.

II. ATTENTION ENHANCED RESERVOIR COMPUTING

A. Reservoir Computing

Reservoir Computing (RC) is a paradigm in the field of recurrent neural networks that offers an efficient approach to tasks involving temporal dynamics and sequential patterns [17]. The delay-based RC is a prime example of RC, distinctive for its utilization of time-multiplexed masking for input representation [12]. Instead of directly feeding the input data $D(t)$ to the system, it is multiplied, element-wise, with a periodic mask $M(t)$, which is essentially a high-dimensional random vector repeated periodically. This mask expands and distributes the input information across the available input span, thus enriching the temporal dynamics of the system. The masked input $v(t)$ is formally represented as $v(t) = D(t) \odot M(t \bmod T)$, where M is the masking vector, T is the period, and \odot represents a D -elementwise multiplication with the

* felixk@mail.saitama-u.ac.jp

† auchida@mail.saitama-u.ac.jp

full M vector. The readouts R in delay-based RC are also time-distributed, capturing the reservoir's response at different time instants within the period T . By sampling the system's response at multiple points across this period, a high-dimensional representation is obtained, allowing for rich and diverse dynamics to be captured for downstream tasks. In this study, we use a mask $m(t)$ that is constant for N intervals of length θ , i.e. $T = N\theta$, where the values of m_n are drawn randomly from a uniform distribution on the interval between 0 and 1.

We use a delay-based photonic reservoir computer, which captures the dynamics of semiconductor lasers with weak optical feedback. The Lang-Kobayashi equations mathematically represent the systems as follows [4, 5, 22].

$$\dot{E}(t) = (1 + i\tilde{\alpha})E(t) - |E(t)|^2E(t) + \eta E(t - \tau) \exp(i\phi) \quad (1)$$

$$\dot{n}(t) = p + \eta v(t) - (1 + |E(t)|^2)n(t) \quad (2)$$

where, $E(t)$ denotes the complex electric field amplitude, $n(t)$ represents the carrier density, $\tilde{\alpha}$ is the linewidth enhancement factor, η signifies the feedback strength, τ is the time delay, ϕ is the phase shift, and p is the normalized injection current.

Within the context of delay-based RC, the input modulates the pump term, thus affecting the system's dynamics. The modulated pump term is denoted as $\eta v(t)$, where η is the input strength and $v(t)$ is the input to the reservoir system. The readouts R are derived from the intensity $|E(t)|^2$ of the electric field amplitude. In the RC framework, only the readout weights W_{out} , which connect the reservoir states to the output, are trained while the internal weights of the reservoir are left unchanged [16]. The output or readout weights are crucial in mapping the reservoir states to the desired outputs. Denoted typically as W_{out} , these weights are applied to the reservoir states R . Training the output weights involves optimizing them to minimize the distance between the approximations $\tilde{U} = W_{\text{out}}R$ and the true target values U . Commonly, a linear regression approach is employed [16], considering a regularization term to prevent overfitting. The training process can be mathematically represented as:

$$W_{\text{out}} = \arg \min_W (||U - WR||^2 + \lambda ||W||^2) \quad (3)$$

where R denotes the collection of reservoir states, U represents the target outputs, and λ is the regularization coefficient.

The analytic solution to the ridge regression problem can be derived by setting the gradient of the objective function with respect to W to zero. The resulting equation can be expressed as:

$$W_{\text{out}} = (RR^T + \lambda I)^{-1}RU^T, \quad (4)$$

where I denotes the identity matrix. This solution provides a direct way to compute the optimal W_{out} without iterative optimization. The addition of the regularization term λI ensures that the matrix $RR^T + \lambda I$ is invertible, thus guaranteeing a unique solution and penalizing overfitting.

Parameter	Numerical Value
Mask period T	$N\theta = 5 \times 10^{-9}$ s
Linewidth enhancement factor $\tilde{\alpha}$	3.01
Phase shift ϕ	0.0
Feedback strength η	10^8
Time delay τ	$1.01T = 5.05 \times 10^{-9}$
Normalized injection current p	1.11
Input strength η	0.08
Number of nodes N	50
Interval length θ	10^{-10} s

Table I. Summary of parameters and their numerical values.

B. Attention Mechanism

In deep learning, particularly when dealing with sequential data, the attention mechanism has emerged as a groundbreaking concept [18]. This mechanism enables models to selectively focus on relevant portions of the input sequence during output generation, mirroring how humans selectively prioritize information during decision-making or data processing. Central to this mechanism is the calculation of attention weights, which subsequently guide a weighted combination of input values. These weights effectively signify the level of "attention" or importance each part of the input should receive.

To clarify the method of attention, we present an example inspired by Ref. [23]. Imagine a database containing daily temperature records over several years, illustrated as tuples such as {"2024-01-01", "-2°C"}, {"2024-01-02", "0°C"}, {"2024-01-03", "3°C"}}, where the dates act as keys (k) and temperatures as values (v). Querying this database (q) with the date "2024-01-02", would fetch the exact temperature "0°C". When an exact match for the queried date is absent and approximate matching is allowed, the system might return approximate temperatures close to neighboring dates.

Expanding on this illustration, we compute a distance function between the query (q) and the keys (k) within the entire dataset $\mathbf{D} = \{(k_1, v_1), \dots, (k_m, v_m)\}$, providing a weighting (or attention) to the associated values (v). This relationship is captured as:

$$\text{attention}(q, K) = \sum_{i=1}^m \alpha(q, k_i) v_i, \quad (5)$$

where $\text{attention}(q, K)$ is the weighted sum of all data points for the given query, i indexes the dataset \mathbf{D} , and $\alpha(q, k_i)$ denotes the scalar attention weights. An interesting aspect is the determination of the function α . Several functions can be employed, from traditional distances like the Boxcar function, defined as $\alpha_{\text{Boxcar}} = 1$ if $||q - k_i|| \leq 1$, to a Gaussian similarity, given by $\alpha_{\text{Gaussian}} = \exp(-||q - k_i||_2^2)$ [23]. In contemporary deep learning, the function α is often approximated using neural networks, allowing gradient descent to tailor the function optimally to the dataset.

A more recent progression in attention mechanisms introduces the concept of self-attention [18, 24]. In this frame-

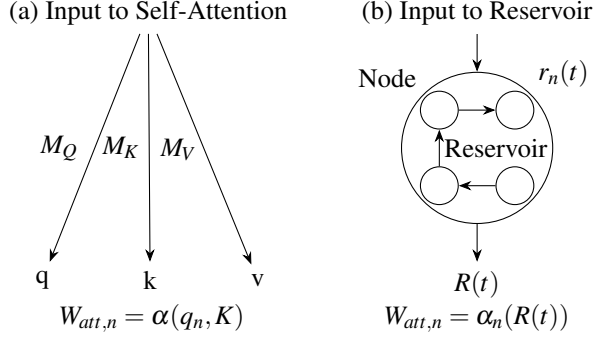


Figure 1. (a): Self-attention mechanism creating queries (q), keys (k), and values (v) from an input. (b): Reservoir approach transforming an input into a high dimensional reservoir state $R(t)$. Both projections are then used in a neural network α to yield the attention weights $W_{att,n}$.

work, the queries (q), keys (k), and values (v) originate from the same data point. For each individual data point (e.g. the temperature at a specific time step), corresponding queries (q), keys (k), and values (v) are produced. Typically, these elements are generated through matrix transformations, where the matrix weights are refined and optimized using a gradient descent algorithm.

C. Incorporation of Attention Layer in Reservoir Computing

Next, we delve into incorporating the attention mechanism within a reservoir computer. This requires a clear understanding of its implementation and the definitions of queries (q), keys (k), and values (v) in the context of reservoir computing. While numerous potential locations for integrating the attention mechanism exist, we focus on its application to improve the reservoir computer's output layer. Therefore we replace the traditional weights W_{out} with the scalars $\alpha(q, k)$.

In our attention-enhanced reservoir computer, the reservoir states r_n simultaneously serve as the queries (q), keys (k), and values (v). This is reminiscent of the self-attention scheme where every data point of the input sequence is projected onto queries (q), keys (k), and values (v), often via matrices learned through a gradient descent algorithm [18, 24]. Consequently, the attention weight associated with a particular reservoir node is expressed as:

$$\tilde{u}(t) = \sum_{n=1}^N W_{att,n}(R(t))r_n(t) = \sum_{n=1}^N \alpha_n(R(t))r_n(t), \quad (6)$$

where $W_{att,n}(R(t))$ is the weight applied to the n -th reservoir node, $R(t) = (r_1(t), \dots, r_N(t))$ denotes the whole reservoir state and $r_n(t)$ is an explicit reservoir state of the n -th node at time t , and the summation spans all N reservoir nodes. Hence, the weight assigned to the reservoir state of the n -th node is given by some transformation α of all N reservoir states. Connecting this to the self-attention mechanism, the reservoir projects the input into a high-dimensional feature

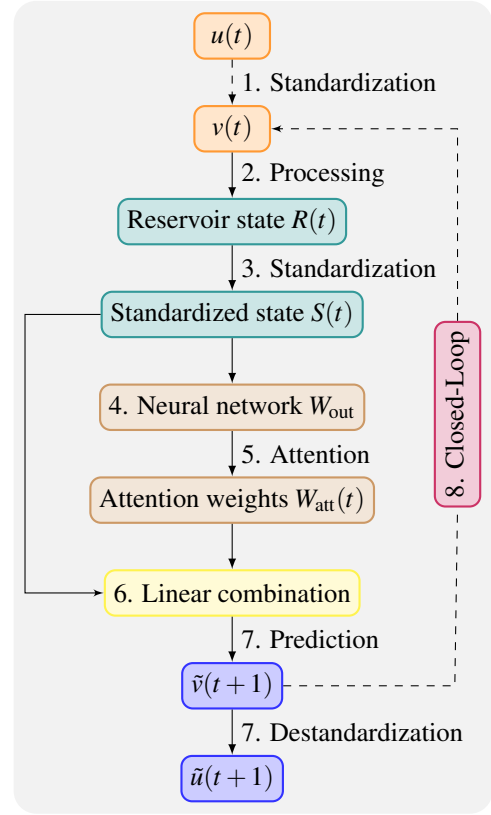


Figure 2. Schematic representation of the reservoir computing process augmented with an attention mechanism.

space, similar to the matrix transformation that projects the input data point to the queries (q), keys (k), and values (v). The side-by-side comparison is shown in Fig. 1. In the self-attention mechanism, the query of a data point combined with the keys of all other data points in the sequence generates the attention weights, which are then weighted with the values. From Eq. (6), the role of all reservoir states $R = (r_1, \dots, r_N)$ in the function α is equal to the queries and the keys of the attention in Eq. (5). The resulting attention weights $W_{att,n}$ are multiplied with the values (v), which in our case are the reservoir states r_n . A sum over all these weighted reservoir states ($W_{att,1}r_1, \dots, W_{att,N}r_N$) then yields the final prediction \tilde{u} . For flexibility and optimization, we allow the function α to be determined by a neural network. In the scope of this paper, this is reduced to a linear transformation, i.e., a tensor. Thus, this simple linear transformation approach can concisely be written as:

$$W_{att}(t) = W_{out}R(t), \quad (7)$$

$$\tilde{u}(t) = W_{att}(t)R(t), \quad (8)$$

where \tilde{u} represents the approximation for the target u of the given task, $W_{att}(t)$ are the time-dependent attention scalar weights, and W_{out} are weights that are trained via a gradient descent algorithm. Thus, to get the attention weight $W_{att,n}(t)$ for the n -th reservoir state r_n , we compute $W_{att,mn}(t) = \sum_{l=1}^N W_{out,mnl}r_l$. Note that W_{out} is a third-order tensor with di-

mensions $\mathbb{R}^{N \times N \times M}$, where N denotes the number of readout nodes in the reservoir, and M represents the dimensionality of the target. This configuration can result in a substantial number of weights for a reservoir of significant size combined with a large target dimension. One potential solution to mitigate this problem is to compute the attention weights using only a subset of accessible nodes, reducing the N term to a smaller n' term, where $n' \ll N$. However, we employ the full node set in our current example with smaller dimensions.

A detailed visualization of our complete scheme is shown in the diagram depicted in Fig. 2. We further unpack this representation by providing a step-by-step explanation of the underlying operations.

1. Data Standardization

Before processing, the raw input data $u(t)$ undergoes a standardization process, ensuring the data is in the optimal state for reservoir processing, not saturating the reservoir state. Standardization ensures that the mean of the data is zero and the standard deviation is one. The outcome, $v(t)$, represents the standardized version of the input data.

2. Reservoir Processing

The standardized data, $v(t)$, is then passed into the reservoir, resulting in a reservoir state, $R(t)$. This reservoir state is an intermediate, high-dimensional representation of the input data.

3. State Standardization

Like the initial data, the reservoir state $R(t)$ is standardized to obtain $S(t)$, the standardized reservoir state. This step ensures that the reservoir state is normalized and ready for the subsequent neural network processing.

4. Neural Network Processing

The standardized reservoir state, $S(t)$, undergoes processing through a neural network with weights W_{out} . Regarding the training of the weights W_{out} , deep learning methods can be applied [25] using a gradient descent algorithm:

$$W_{\text{out}}(n+1) = W_{\text{out}}(n) - \gamma \nabla F(W_{\text{out}}(n), S), \quad (9)$$

with γ being a learning rate, which we set to 0.01, and n iterates through the gradient descent epochs, and the optimization objective is:

$$W_{\text{out}} = \min_W (F(W, S, U)), \quad (10)$$

where S is the set of all reservoir states and U is the target dataset. We deploy as F a simple squared distance, i.e.

$F(W, S, U) = \frac{1}{2} \|\tilde{U}(S, W) - U\|_2^2$, with $\tilde{U}(S, W)$ being the approximation to the target dataset U .

The attention-enhanced reservoir thus loses its advantage of utilizing the analytically solvable ridge regression as an optimization approach. Owing to the recent improvement in hardware-accelerated optimization of gradient descent approaches, we believe that the limiting computation factor of reservoir computing is not the output layer optimization. Therefore, augmenting reservoir computing with the attention mechanism could couple the best of two worlds.

5. Attention Mechanism

The attention weights, $W_{\text{att}}(t)$, emerge from the neural network. These weights dictate how much importance is placed on each node or neuron in the reservoir at a specific time. In essence, the attention mechanism dynamically adjusts, prioritizing certain nodes over others based on their relevance to the output at that particular time step.

A broad range of possible neural networks can be selected. This study focuses on the simplest approach by adding a linear attention layer to the delay-based reservoir computing setup. The attention weights $W_{\text{att}}(t)$ are computed via a linear transformation of the standardized reservoir state $S(t)$ via the weights W_{out} , represented as:

$$W_{\text{att}}(t) = W_{\text{out}} S(t) \quad (11)$$

6. Linear Combination

The attention weights and the standardized reservoir states are then linearly combined. This combination effectively amplifies the states that the attention mechanism deems significant while reducing the others. The corresponding prediction output $\tilde{v}(t+1)$ is given by:

$$\tilde{v}(t+1) = W_{\text{att}}(t) S(t) \quad (12)$$

7. Prediction and Destandardization

The linear combination yields a prediction $\tilde{v}(t+1)$, which is subsequently destandardized to produce the output $\tilde{u}(t+1)$. This output represents the forecasted value of the time series.

Our integration of the attention layer in reservoir computing enables the system to prioritize important features in the input data, particularly in complex time series forecasting scenarios. By dynamically shifting focus to the most important nodes in the reservoir based on context, the attention-enhanced reservoir computer offers a more nuanced and accurate representation of the data.

D. Prediction Quality Metrics

In the context of reservoir computing for time series forecasting, two primary configurations are commonly used: the open-loop and closed-loop [26].

1. Normalized Root Mean Square Error

In the open-loop configuration, the model performs a one-step-ahead predictions. We evaluate the model's prediction accuracy via the normalized root mean square error (NRMSE) [27]:

$$\text{NRMSE} = \sqrt{\frac{\sum_{l=1}^L \|u_l - \tilde{u}_l\|^2}{N\text{Var}(u)}}, \quad (13)$$

where u_l is the l -th target data point, \tilde{u}_l is the prediction data, l is the index up to the L -th data point, and $\text{Var}(u)$ is the variance over the whole data set.

2. Valid Prediction Time

Fig. 2 illustrates the closed-loop feedback configuration. In this setup, after the model has been trained, it is switched to a closed-loop mode, where the model's own predictions are recursively fed back as input. This method allows for continuous predictions, extending beyond the one-step-ahead prediction. The quality of predictions in a closed-loop configuration is evaluated by a metric called the valid prediction time (VPT) [28], defined as:

$$\text{VPT} = \delta_u(t) > 0.4, \quad \delta_u(t) = \frac{|u(t) - \tilde{u}(t)|^2}{\langle |u(t) - \langle u(t) \rangle|^2 \rangle}, \quad (14)$$

where VPT measures the first time at which $\delta_u(t)$ surpasses the value of 0.4, in which $\delta_u(t)$ measures the average normalized distance over the trajectory between the true system $u(t)$, the approximation \tilde{u} , and $\langle \rangle$ denotes the time average. VPT measures the duration for which the model's predictions remain within an acceptable error threshold, thereby indicating the effectiveness of the model in maintaining reliable forecasts over time. Unlike open-loop predictions, closed-loop predictions compound potential errors over time, because of the sensitive dependence on initial conditions on chaotic dynamic systems.

III. NUMERICAL RESULTS

This section presents the comparative results of the attention-enhanced photonic reservoir computing method to the conventional linear regression technique. The evaluation is performed for a unidirectionally-coupled two-Lorenz system introduced in Sec. III A and a Lorenz-Rössler system introduced in Sec. III B.

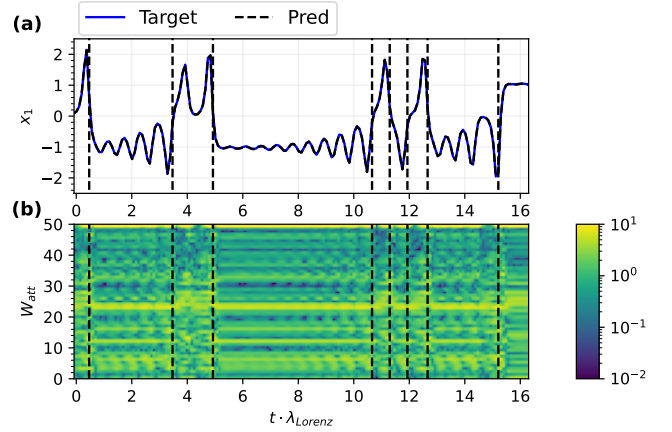


Figure 3. Example time series of open-loop configuration for the UCTLS. The upper graph shows the x -variable of the time series, while the lower graph shows the attention weights in the same time interval for a 50-node reservoir. The dashed black lines indicate a shift from the attractor, pinpointing the dynamical adjustment of the weights to the task.

A. Unidirectionally-Coupled Two-Lorenz System (UCTLS)

1. Model

As a benchmark task, we utilize a unidirectionally-coupled two-Lorenz system (UCTLS) [20, 29], defined by the following equations:

$$\dot{x}_1 = (a + \sigma_{\text{force}x_2})(y_1 - x_1), \quad (15)$$

$$\dot{y}_1 = x_1(b + \sigma_{\text{force}y_2} - z_1) - y_1, \quad (16)$$

$$\dot{z}_1 = x_1y_1 - (c + \sigma_{\text{force}z_2})z_1, \quad (17)$$

$$\dot{x}_2 = a(y_2 - x_2), \quad (18)$$

$$\dot{y}_2 = x_2(b - z_2) - y_2, \quad (19)$$

$$\dot{z}_2 = x_2y_2 - cz_2. \quad (20)$$

These equations represent two Lorenz systems, with the first one being driven by the second. The parameters used, namely $a = 10$, $b = 28$, and $c = \frac{8}{3}$, are the standard Lorenz parameters [20]. The key distinction is the introduction of a forcing term, σ_{force} , that couples the two systems unidirectionally.

For the reservoir computing task, only the x_1 , y_1 , and z_1 variables are exposed, while x_2 , y_2 , and z_2 are hidden. Predicting such a non-markovian deterministic chaotic time series is challenging [30], especially when it has underlying hidden states that are not directly observable by the reservoir computer. The system was integrated with a Runge-Kutta 45-step approach with a step size of $dt = 0.01$, while the sampling time is $dt_{\text{sample}} = 0.1$. Regarding the largest Lyapunov exponent of the system, our simulations indicate that no significant variation up to a force of $\sigma_{\text{force}} = 0.15$ is exhibited relative to the classic Lorenz value of $\lambda_{\text{Lorenz}} \approx 0.91$. For all simulations we use 25000 training and 5000 testing data points.

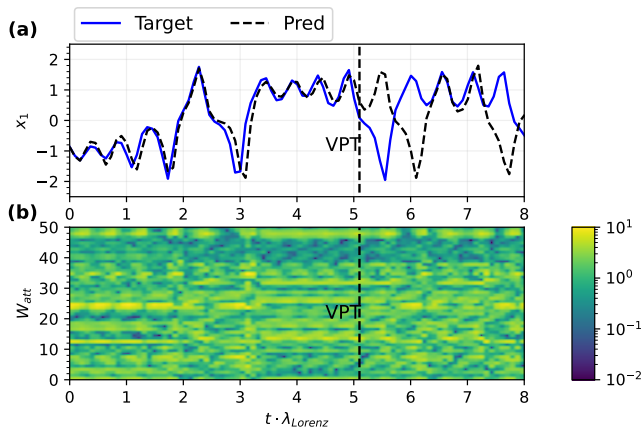


Figure 4. Closed loop time series of a UCTLS for a 50-node reservoir. The true trajectory and closed loop prediction are depicted by the solid blue and dashed black lines, respectively. The color bar shows the magnitude of the attention weights. The vertical dashed black line indicates the time point for VPT computation.

We begin with the UCTLS as defined by Eqs. (15)-(20) subjected to a perturbation strength of $\sigma_{\text{force}} = 0.05$, implemented in a photonic reservoir utilizing 50 nodes, with other parameters specified in Table 1.

2. Results of Time Series and Weights

Fig. 3(a) illustrates an open-loop time series. The upper graph displays the time series of the x_1 -variable from the second Lorenz attractor of the true system (in blue) alongside the predicted time series (dashed black line), plotted against the time in Lyapunov times with $\lambda_{\text{Lorenz}} \approx 0.91$. The similarity between the prediction and the actual system's behavior is accurate.

A more interesting insight comes from Fig. 3(b), which shows the computed attention weights for each node within the reservoir across the same period. Nodes with higher weight magnitudes are assumed to be more important for predictions at specific time points. Vertical dashed lines indicate a pattern change corresponding to moments where the system's trajectory shifts from one side of the attractor to the other. A corresponding shift in the attention weights' structure implies that the attention-augmented reservoir can adapt dynamically to the time-dependent characteristics of the task. This feature is essential, as the UCTLS demands time-dependent transformations depending on the current position within the attractor space.

The attention mechanism provides a dynamic adjustment unlike the static nature of weights employed in linear regression, which cannot distinguish this characteristic. Given that nearly all complex systems evolve with time, adaptively adjusting the significance of different nodes is not just beneficial but necessary. This strongly illustrates the inherent limitations of static approaches when dealing with systems characterized by dynamic evolution.

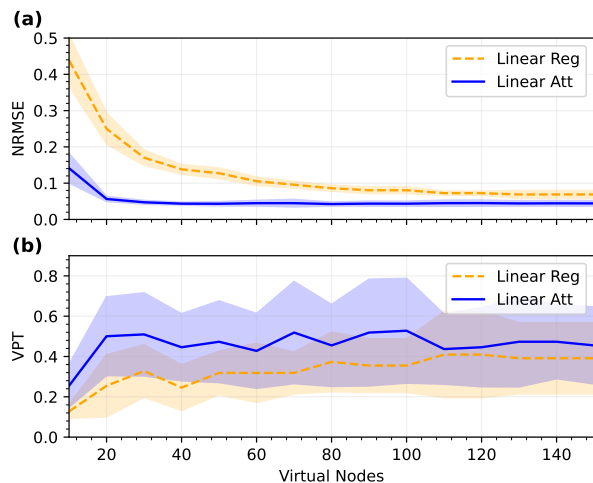


Figure 5. Comparison of VPT and NRMSE for classical linear regression (dashed orange line) and attention-enhanced reservoir computing (solid blue line) with varying reservoir size N of UCTLS.

This behavior continues even if the closed-loop configuration is applied, as shown in Fig. 4. The reservoir's prediction and the true trajectory stay close to each other until around 5 Lyapunov times, indicated by a vertical dashed black line pinpointing to the time at which the VPT (see Sec. II D) is computed. The weights in the lower graph show the distinctive feature of adjusting to the dynamical problem itself despite being configured in the closed-loop scheme.

3. Results of Quality Metrics

To showcase the efficacy of dynamic adjustment, we simulated an ensemble prediction across ten distinct trajectories for varying reservoir sizes. The results are shown in Fig. 5. We computed the NRMSE for the open loop depicted in Fig. 5(a) and the VPT for the closed loop illustrated in Fig. 5(b). These metrics were calculated for both the classical linear regression model (dashed orange line) and the attention-augmented model (solid blue line) across a spectrum of reservoir sizes, from 10 to 150 nodes.

The results indicate that the attention-augmented model yields a lower NRMSE for smaller-sized reservoirs while simultaneously achieving a higher VPT. Although this advantage diminishes as the reservoir size increases, it stays consistent. Notably, the optimal performance of the attention-enhanced reservoir is observed with as few as 20 nodes. This suggests that the attention mechanism significantly reduces the required size of the reservoir. However, this size reduction comes at the costs of additional weights in the output layer. Nonetheless, this approach is particularly interesting when only limited reservoir sizes are realistically accessible.

We analyze the average power spectrum of a reservoir with 20 nodes, reproducing the UCTLS task with $\sigma_{\text{force}} = 0.05$. Fig. 6 displays the resulting spectra: the true system's spec-

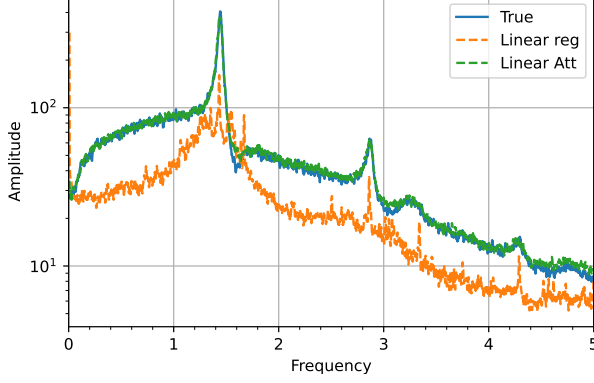


Figure 6. The Fourier Spectrum of a predicted time series in the closed-loop configuration with a reservoir size of $N = 30$. The true system is depicted as a solid blue line, while the classic linear regression and the attention enhanced reservoir are shown as dashed orange and green lines respectively

trum is depicted by the blue curve, the orange curve represents the closed-loop outcome of the classical linear regression approach, while the green curve corresponds to the linear attention approach.

An examination of Fig. 6 reveals that the linear regression approach significantly deviates in reconstructing the spectrum of the original attractor, failing to identify the correct main frequency and the secondary peak at a frequency of 2.9Hz. In contrast, the linear attention method successfully captures both frequencies, reproducing very accurately the power spectrum.

To deepen our analysis of the UCTLS, we evaluate the dependency of the NRMSE and VPT on the driving force σ_{force} . We keep the reservoir size constant with $N = 50$ nodes, while the other parameters are unchanged. The results are illustrated in Fig. 7, using the same color coding and line style as in Fig. 5. The behavior of the classic single Lorenz system is represented on the left side of the graph with a driving force of $\sigma_{\text{force}} = 0$. The linear attention method outperforms the classical linear regression approach for the VPT and NRMSE metrics in this regime.

When the forcing strength is increased, the observed improvement for VPT diminishes, while the NRMSE gradually increases for both methods. However, the attention-enhanced approach yields lower NRMSE values throughout. These results underline the improved predictive performance of the attention-enhanced reservoir relative to the traditional approach.

B. Alternating Lorenz and Rössler System (ALRS)

1. Model

The second benchmark is a target dataset constructed using two canonical chaotic systems: the Rössler and Lorenz mod-

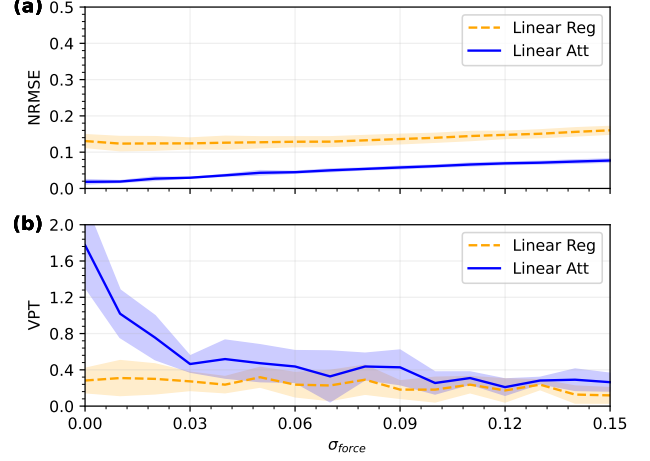


Figure 7. Mean over ten trajectories of the the VPT and NRMSE for classical linear regression (dashed orange line) and attention enhanced reservoir computing (solid blue line) with varying coupling strength σ_{force} of UCTLS. The shaded areas depict the standard deviation. The photonic reservoir size was set to $N = 50$ nodes.

els [31]. For the Rössler model, the equations of motion are given by:

$$\frac{dx_R}{dt} = -y_R - z_R, \quad (21)$$

$$\frac{dy_R}{dt} = x_R + a_R y_R, \quad (22)$$

$$\frac{dz_R}{dt} = b_R + x_R z_R - c_R z_R. \quad (23)$$

For the Lorenz model, the dynamics are described by:

$$\frac{dx_L}{dt} = a_L(y_L - x_L), \quad (24)$$

$$\frac{dy_L}{dt} = -x_L z_L + b_L x_L - y_L, \quad (25)$$

$$\frac{dz_L}{dt} = x_L y_L - c_L z_L. \quad (26)$$

The parameters used in our simulations are $a_R = 0.2, b_R = 0.2, c_R = -5.7$ for the Rössler system and $a_L = 10, b_L = 28, c_L = -\frac{8}{3}$ for the Lorenz system. Both these systems are known for generating deterministic chaos. For data generation, we exclusively consider the x -variable trajectories (x_R for Rössler and x_L for Lorenz) if the open loop configuration is applied, while for the closed loop configuration the x, y, z variables are exposed. The Rössler system is integrated with a time step of $dt = 0.05$, while every ten points are downsampled in an effective time step of $dt_{\text{sample}} = 0.5$. Similarly, the Lorenz system was integrated using a time step of $dt = 0.01$ and subsequently downsampled to achieve an effective time step of $dt_{\text{sample}} = 0.1$. For each system, multiple 500-step trajectories are generated. These trajectories are then alternatively concatenated, yielding a time series that alternates be-

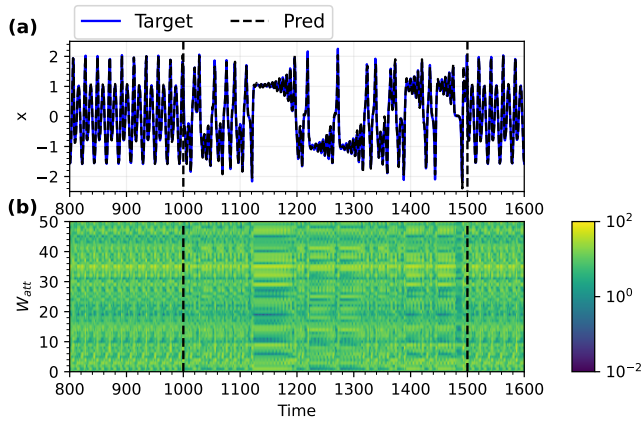


Figure 8. Example time series of open-loop configuration for ALRS. The upper graph shows the x -variable of the time series, while the lower graph shows the attention weights in the same time interval. The dashed black lines indicate the change in task from Rössler to Lorenz or vice versa, pinpointing to the dynamical adjustment of the weights to the task.

tween Rössler and Lorenz every 500 points for 25000 training data points and 5000 testing data points [31]. Before concatenation, the time series data from both models are standardized to ensure zero mean and unit standard deviation. We call this benchmark the ALRS. For both systems, the largest Lyapunov exponents are calculated with $\lambda_{\text{Lorenz}} \approx 0.91$ and $\lambda_{\text{Rössler}} \approx 0.071$. For all simulations, we use 25000 training and 5000 test data points.

2. Results

We investigate the ALRS, defined by Eqs. (21) to (26) in the same manner. An exemplary time series for this system is depicted in Fig. 8. Fig. 8(a) indicates that the prediction closely approximates the true system, suggesting a high degree of accuracy in forecasting the next state.

Fig. 8(b) provides the interesting part of the attention-enhanced reservoir. The vertical dashed lines denote the transitions between the Lorenz and Rössler dynamics within the task. A shift in the attention weights in response to these changes can be observed, implying that the attention-enhanced reservoir can adapt to different dynamical problems presented by the input signal.

To quantitatively analyze the prediction quality, we computed the NRMSE for the open loop and the VPT for the closed loop in ALRS across reservoir sizes, spanning from 10 to 150 nodes, as shown in Fig. 9. Note that in the ALRS benchmark, two different VPTs are computed by starting the closed loop configuration either in a window of Rössler inputs or in a window of Lorenz inputs. Here, the NRMSE for the classical linear regression method is presented by the dashed orange line, while the solid blue line represents the attention-based approach. These findings agree with previous observations: the attention-enhanced reservoir yields smaller NRMSE (higher VPT), with the effect being particularly pronounced

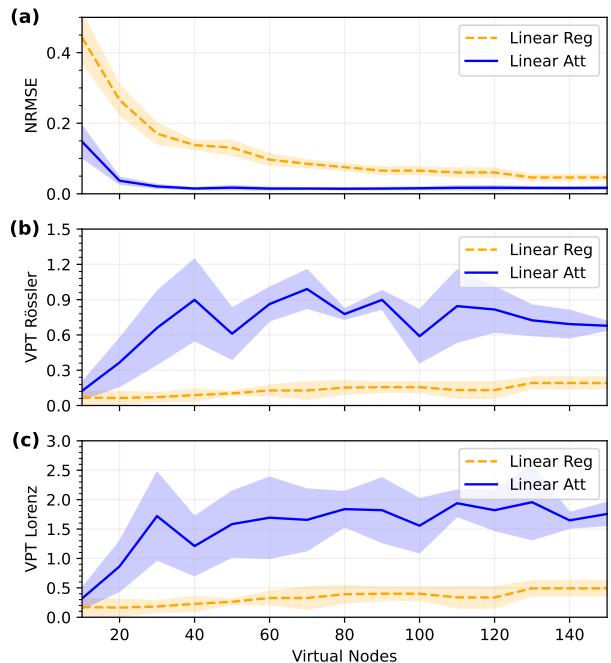


Figure 9. NRMSE of the open loop task and VPTs of the closed loop configuration for the ALRS over the reservoir size N . The mean of ten trajectories for the classic linear regression is shown as a dashed orange line, while the attention-enhanced reservoir approach is depicted as a solid blue line. The shaded areas are the standard deviation.

for smaller reservoir sizes. Interestingly that this dynamic adjustment can tackle a problem that swiftly changes between two distinct attractors.

Finally, we analyze the NRMSE for predicting more than one step ahead for the UCTLS and ALRS [8]. The results are shown in Fig. 10, depicting the NRMSE over k -steps for future predictions. The UCTLS system was simulated with a driving force of $\sigma_{\text{force}} = 0.05$. Both reservoirs for the UCTLS and ALRS tasks utilize 50 nodes. The dashed orange line shows the classical ridge regression approach while the solid blue line depicts the attention-enhanced scheme. The improvement for the UCTLS case is clear for all prediction steps into the future, decreasing the NRMSE by a small amount. More impressively, the NRMSE decreases for the ALRS approach in the lower graph, where a significant reduction in the NRMSE is clearly observed.

IV. CONCLUSION

We introduced an attention mechanism to reservoir computing to demonstrate a notable improvement predicting complex dynamical systems. Across our simulations of the UCTLS and ALRS, the attention-enhanced reservoir consistently out-

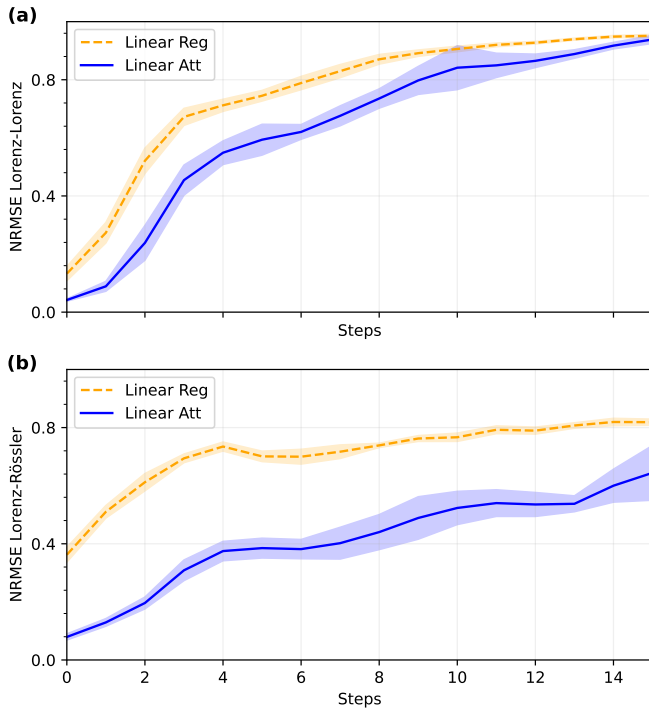


Figure 10. NRMSE of the open loop task for the UCTLS and the ALRS system over the number of steps k to predict into the future. The mean of ten trajectories for the classic linear regression is shown as a dashed orange line, while the attention-enhanced reservoir approach is depicted as a solid blue line. The shaded areas represent the standard deviation.

performed classical linear regression methods. It has shown particular advantages in scenarios with smaller reservoir sizes, indicating its potential to reduce system requirements without sacrificing performance but at the cost of an attention layer.

This study highlights the importance of dynamically-adjustable weights, characteristics of the attention mechanism, and their effect in predicting the complex behaviors of nonlinear dynamic systems. Notably, the attention-enhanced reservoir exhibits swift adaptability to sudden changes in dynamic input, a quality that promises significant improvements in real-time applications. By achieving lower prediction errors and capturing key spectral features more accurately, the attention-enhanced approach provides an efficient method for integrating attention within various reservoir computing schemes.

ACKNOWLEDGMENTS

This study was partly supported by JSPS KAKENHI (JP19H00868, JP20K15185, JP22H05195). We thank Ryugo Iwami, André Röhm, and Dhruvit Patel for productive discussions.

- [1] Y. Shen, N. C. Harris, S. Skirlo, M. Prabhu, T. Baehr-Jones, M. Hochberg, X. Sun, S. Zhao, H. Larochelle, D. Englund, and M. Soljačić, Deep learning with coherent nanophotonic circuits, *Nature Photonics* **11**, 441 (2017).
- [2] L. Larger, M. C. Soriano, D. Brunner, L. Appeltant, J. M. Gutiérrez, L. Pesquera, C. R. Mirasso, and I. Fischer, Photonic information processing beyond turing: an optoelectronic implementation of reservoir computing, *Optics Express* **20**, 3241 (2012).
- [3] M. Nakajima, K. Tanaka, and T. Hashimoto, Scalable reservoir computing on coherent linear photonic processor, *Communications Physics* **4**, 20 (2021).
- [4] D. Brunner, M. C. Soriano, C. R. Mirasso, and I. Fischer, Parallel photonic information processing at gigabyte per second data rates using transient states, *Nature Communications* **4** (2013).
- [5] J. Nakayama, K. Kanno, and A. Uchida, Laser dynamical reservoir computing with consistency: an approach of a chaos mask signal, *Optics Express* **24**, 8679 (2016).
- [6] J. Bueno, D. Brunner, M. C. Soriano, and I. Fischer, Conditions for reservoir computing performance using semiconductor lasers with delayed optical feedback, *Optics Express* **25**, 2401 (2017).
- [7] C. Sugano, K. Kanno, and A. Uchida, Reservoir computing using multiple lasers with feedback on a photonic integrated circuit, *IEEE Journal of Selected Topics in Quantum Electronics* **26**, 1 (2020).
- [8] K. Takano, C. Sugano, M. Inubushi, K. Yoshimura, S. Sunada, K. Kanno, and A. Uchida, Compact reservoir computing with a photonic integrated circuit, *Optics Express* **26**, 29424 (2018).
- [9] S. Sackesyn, C. Ma, J. Dambre, and P. Bienstman, Experimental realization of integrated photonic reservoir computing for nonlinear fiber distortion compensation, *Optics Express* **29**, 30991 (2021).
- [10] M. Rafayelyan, J. Dong, Y. Tan, F. Krzakala, and S. Gigan, Large-scale optical reservoir computing for spatiotemporal chaotic systems prediction, *Physical Review X* **10**, 041037 (2020).
- [11] S. H. Strogatz, *Nonlinear Dynamics and Chaos: With Applications to Physics, Biology, Chemistry and Engineering* (Westview Press, 2000).
- [12] L. Appeltant, M. C. Soriano, G. Van der Sande, J. Danckaert, S. Massar, J. Dambre, B. Schrauwen, C. R. Mirasso, and I. Fischer, Information processing using a single dynamical node as complex system, *Nature Communications* **2**, 468 (2011).
- [13] J. Torrejon, M. Riou, F. A. Araujo, S. Tsunegi, G. Khalsa, D. Querlioz, P. Bortolotti, V. Cros, A. Fukushima, H. Kubota, S. Yuasa, M. D. Stiles, and J. Grollier, Neuromorphic computing with nanoscale spintronic oscillators (2017), arXiv:1701.07715 [cs.ET].
- [14] K. Nakajima, H. Hauser, T. Li, and R. Pfeifer, Information processing via physical soft body, *Scientific Reports* **5**, 10.1038/srep10487 (2015).

- [15] T. Kotooka, S. Lilak, A. Stieg, J. Gimzewski, N. Sugiyama, Y. Tanaka, H. Tamukoh, Y. Usami, and H. Tanaka, Ag2se nanowire network as an effective in-materio reservoir computing device (2021), preprint, not peer-reviewed, ResearchSquare:10.21203/rs.3.rs-322405/v1.
- [16] H. Jaeger, The “echo state” approach to analysing and training recurrent neural networks—with an erratum note, Bonn, Germany: German National Research Center for Information Technology GMD Technical Report **148**, 13 (2001).
- [17] G. Tanaka, T. Yamane, J. A. He, R. Nakane, S. Kanazawa, H. Takeda, H. Numata, D. Nakano, and A. Fujii, Recent advances in physical reservoir computing, *Neural Networks* **115**, 100 (2019).
- [18] A. Vaswani, N. Shazeer, N. Parmar, J. Uszkoreit, L. Jones, A. N. Gomez, Ł. Kaiser, and I. Polosukhin, Attention is all you need, in *Advances in neural information processing systems* (2017) pp. 5998–6008.
- [19] S. Bai, J. Z. Kolter, and V. Koltun, An empirical evaluation of generic convolutional and recurrent networks for sequence modeling, arXiv preprint arXiv:1803.01271 (2018).
- [20] E. N. Lorenz, Deterministic nonperiodic flow, *Journal of Atmospheric Sciences* **20**, 130 (1963).
- [21] E. Igra, Knots and chaos in the rössler system (2023), arXiv:2306.04772 [math.DS].
- [22] A. Uchida, Optical communication with chaotic lasers: Applications of nonlinear dynamics and synchronization (1994).
- [23] A. Zhang, Z. C. Lipton, M. Li, and A. J. Smola, *Dive into Deep Learning* (Cambridge University Press, 2023) <https://D2L.ai>.
- [24] D. Bahdanau, K. Cho, and Y. Bengio, Neural machine translation by jointly learning to align and translate, arXiv preprint arXiv:1409.0473 (2014).
- [25] I. Goodfellow, Y. Bengio, and A. Courville, *Deep learning* (MIT press, 2016).
- [26] M. Cucchi, S. Abreu, G. Ciccone, D. Brunner, and H. Kleemann, Hands-on reservoir computing: a tutorial for practical implementation, *Neuromorphic Computing and Engineering* **2**, 032002 (2022).
- [27] G. James, D. Witten, T. Hastie, and R. Tibshirani, *An introduction to statistical learning: with applications in R* (Springer, New York, 2013) xiv, 426 pages: illustrations (some color); 24 cm.
- [28] J. Pathak, B. Hunt, M. Girvan, Z. Lu, and E. Ott, Model-free prediction of large spatiotemporally chaotic systems from data: A reservoir computing approach, *Physical Review Letters* **120**, 024102 (2018).
- [29] M. O. Fen, Persistence of chaos in coupled lorenz systems, *Chaos, Solitons & Fractals* **95**, 200 (2017).
- [30] H. D. Abarbanel, R. Brown, J. J. Sidorowich, and L. S. Tsimring, The analysis of observed chaotic data in physical systems, *Reviews of Modern Physics* **65**, 1331 (1993).
- [31] K. Kanno, M. Naruse, and A. Uchida, Adaptive model selection in photonic reservoir computing by reinforcement learning, *Scientific Reports* **10** (2020).